Biointerface Research in Applied Chemistry
Open-Access Journal (ISSN: 2069-5837)

Article
Volume 13, Issue 4, 2023, 339
https://doi.org/10.33263/BRIAC134.339

Mullite Ceramics Derived from Fly Ash Powder by Using Albumin as an Organic Gelling Agent

Romit Roy, Dipankar Das [1], Prasanta Kumar Rout [1,*]

[1] Department of Material Science and Engineering, Tripura University (A Central University), Suryamaninagar, Agartala, Tripura, India-799022
* Correspondence: prasantarout@tripurauniv.ac.in (P.K.R);

Scopus Author ID 56085442200
Received: 3.05.2022; Accepted: 3.06.2022; Published: 11.09.2022

Abstract: Mullite is a combination compound of alumina (Al_2O_3) and silica (SiO_2). During the last two decades, mullite ceramics have become the crucial oxide material for both traditional and advanced applications due to their favorable properties, such as good strength at very high temperatures, low density, good thermal shock resistance, and chemically stable. Mullite is also known for its stoichiometry $3Al_2O_3.2SiO_2$, or sometimes it is called 3/2 mullite. In this present investigation, the authors attempt to fabricate mullite-based ceramic through a gel casting process by using an organic binder (egg white) to consolidate powder particles, followed by low-temperature sintering. Fly ash powder, china clay powder, and alumina powder were used as raw materials to make mullite ceramic. Green bodies were fabricated by taking various proportions of fly ash, china clay, and alumina, followed by sintering at 1200°C, 1250°C, and 1300°C for 2 hours. The stability of slurries was studied by measuring zeta potential, and green sample fracture surfaces were analyzed by Field Emission Scanning Electron Microscopy (FESEM). Physical properties of sintered samples, such as linear shrinkage, density, porosity, and water absorption, were also calculated. Evidence of mullite formation was characterized by Field Emission Scanning Electron Microscopy (FESEM scanning electron microscopy (SEM) techniques. The samples containing 45 wt.% fly ash, 15 wt.% china clay, and 40 wt.% aluminas showed the best physical properties compared to other batch compositions and were well supported by the results obtained from FESEM results.

Keywords: mullite; albumin gel casting; zeta potential; fly ash powder; sintering.

1. Introduction

Mullite ($3Al_2O_3.2SiO_2$) is a stable compound that utilizes alumina-silica as raw material for various refractory applications [1,2]. The crystal structure of mullite is orthorhombic, in which the [AlO_6] octahedra and the [SiO_4] share alternate corners and form a three-dimensional framework [3,4]. It has some superior properties like high hot strength, good creep resistance, low dielectric constant and thermal conductivity, good thermal shock resistance, and radiation damage resistance [5]. For that reason, it is considered an attractive material for structural and functional applications such as advanced refractories, crucibles, heat exchangers, hot gas filters, dental ceramic components, fibers, rotary kiln seals, electrical insulation, thermocouple tubes, high-temperature composite, lightweight, fireproof heat insulation components, etc. [3]. Mullite is rarely found in nature, so it has to be prepared or synthesized artificially rather than excavated. Mullite can be fabricated by the sintering method, fusion method, and advanced processing techniques like CDV, spray pyrolysis, sol-gel process, etc. [6]. The starting

materials for the preparation of mullite can be any source of alumina and silica, either in pure form or impure form. Various authors have investigated the preparation, testing, and characterization of mullite ceramics from several available natural mineral materials, such as kaolinite [7], sillimanite group (sillimanite, andalusite, kyanite) [8, 9], staurolite, and topaz [10] and industrial solid waste powder like fly ash [11], bauxite [12], silica fume [13], red mud [14], tincalconite [15], colemanite [16], etc. As per the data available in the literature, although mullite is synthesized by taking various aluminosilicate source materials, fly ash remains the most economical and cost-effective way to fabricate mullite ceramics.

Fly ash is one of the industrial solid wastes generated from coal-based thermal power plants. It contains mainly silica and alumina with some minor oxides present in lesser amounts, namely CaO, Fe_2O_3, MgO, K_2O, Na_2O, TiO_2, etc. [17]. Research activities on the utilization of fly ash are mainly in the construction sector [18], agriculture sector [19], and for making glass and ceramic materials [20], geopolymer [21–23], zeolite [24], etc. Over the last couple of decades, there has been a great effort in preparing mullite ceramic by utilizing fly ash to save natural resources, reduce solid waste, and, more importantly, minimize environmental pollution.

Suriyanarayanan *et al*. [25] synthesized mullite glass ceramics from coal-based thermal industrial waste fly ash and alumina with varying compositions (75:25, 50:50, 25:75) at very high temperatures. It has been reported that a 50:50 weight percentage of coal fly ash and alumina is required for single-phase mullite with complete homogeneity. The single-phase mullitization occurs at the temperature of 920°C. Jung *et al*. [26] synthesized mullite ceramics with a very low porosity of 2.1% by reaction sintering at a temperature of 1500°C, using appropriate mixtures of coal fly ash and alumina powders. 3Y-PSZ powders are used to inhibit the growth of mullite grains and result in good fracture toughness. Hongbin Tan [27] synthesized mullite whiskers by sintering an appropriate mixture of coal fly ash and aluminum sulfate with sodium sulfate as a fluxing agent, where Al_2O_3/SiO_2 molar ratio of 1.5 and sintering temperature is 1000°C for three hours. Dong *et al*. [28] used fly ash and aluminum chloride to synthesize porous mullite ceramics using a heterogeneous precipitation technique. Dong et al. used fly ash powders, bauxite, and magnesium oxide were used for mullite synthesis by Dong et al. [28], where the sintering temperature was between 1500°C to 1550°C. The addition of magnesium oxide enhances densification during the sintering process. Coal fly ash-based mullite powders are prepared by the mullitization, hydrothermal process where boehmite sol is added separately. 12% of boehmite addition at the temperature of 1200°C gives optimum mullite powders [29]. Mondal *et al*. [30] used coal fly ash and bauxite to synthesize alumina and mullite-based composites where the ratio of alumina and silica are kept at 1.5:1, 1.75:1, and 2:1. Sintering temperature results in an increase in density. Cao *et al*. [31] successfully fabricated porous mullite consisting of dense, interlocking rod-like crystals obtained at the sintering temperature of 1500°C from fly ash, bauxite, V_2O_5, and AlF_3. Ma *et al*. [32] prepare prismatic mullite with better crystal interlocking by taking fly ash, bauxite, feldspar, SiC, and V_2O_5, then sintering the sample at 1550 °C. Lath-like mullite crystals were prepared by Yadav *et al*. from fly ash and bauxite, and the samples were fired at 1450°C, resulting in a bulk density obtained 2100 $kg.m^3$ and apparent porosity of 32% [31]. Another researcher, Li *et al*. [29], prepared mullite with fly ash and Boehmite sol; optimal mullite content achieved 63.8% with 12 wt.% boehmites at 1200°C.

There are various reports published about the preparation of mullite ceramics by using fly ash as a raw material. Most of the researchers are using pressing techniques to prepare dense mullite ceramics. There are myriad constraints to the pressing method used to prepare dense mullite ceramics because of high-cost equipment, the tendency to crack in the green body, the limitations of one's arbitrary design, and improper composition and density throughout the cross-section. There could be a possibility that the albumin gel casting process can overcome all these obstacles.

Gel casting was first developed at Oak Ridge National Laboratory (ORNL), Tennessee, USA, in 1991 [34]. It has been used to consolidate various ceramic powders such as Al_2O_3 [35], ZrO_2 [36], SiC [37], SiO_2 [38], $PbZrTiO_3$ [39], etc. Gel casting is one type of colloidal ceramic processing method where the ceramic powder is dispersed in a monomer solution followed by casting into a nonporous mold, where monomers get polymerized by heat or by the addition of certain chemicals and finally form a rigid and homogenous structure by entrapping ceramic particles in the polymeric gel. Various researchers have reported that gel cast slurries include ceramic powders, monomers, initiators, catalyzers, and different additives. Different monomer systems are used in gel casting like acrylamide [39], isobam-104 [41], tertiary-butyl alcohol [42], polyvinyl alcohol (PVA) [43], etc. However, all these monomer systems required a cross-linker, initiator, and catalyst. But other published literature revealed that some natural polymers are used as gelling agents, such as agar [35], alginate [44], agarose [45], gelatin [46], starch [47], albumin [48], etc., which are non-toxic and not required additional cross-linker, initiator, and catalyst. The process allows fabricating complex engineering components with near-net accuracy, high density, and good material homogeneity in green bodies with sufficient strength for handling and machining. The gel casting process has been successfully applied to fabricate both dense wells as porous ceramic components. As per the various literature, it has been found that this method is very much suitable for making structural ceramic, electronic ceramic [49], magnetic ceramics [50], and bio-ceramics [51], as well.

As per the literature survey by the authors, there are a number of literature pieces available related to the fabrication of porous and fibrous mullite ceramic by the gel casting method. Research and development on dense mullite ceramics via gel casting process is very limited. Over the last couple of decades, there has been a great effort in preparing mullite ceramic by utilizing fly ash to save natural resources, reduce solid waste, and, more importantly, minimize environmental pollution. Thus, the current examination aims to investigate fly ash's usage and prepare dense mullite ceramics through an albumin gel casting process.

2. Materials and Methods

2.1. Starting raw materials

In this present work, raw materials such as fly ash powders are obtained from the National Thermal Power Corporation Limited, Bongaigaon, Assam, India, and china clay and alumina are collected from the Ants Ceramics Private Limited, Maharashtra, India, for the synthesis of mullite ceramic. The representative elemental composition of fly ash, china clay, and alumina is analyzed using X-ray fluorescence spectroscopy (Model: AXIOS, make: PANalytical) in Table 1. The raw materials' morphological study was done using Carl Zeiss make field emission scanning electron microscope.

Table 1. Chemical compositions of raw materials.

Oxide Constituents	Raw Materials		
	Fly Ash (wt.%)	China Clay (wt.%)	Alumina (wt.%)
Al_2O_3	55.6	34.67	98.20
SiO_2	29.8	60.53	0.74
CaO	1.59	0.31	0.27
Fe_2O_3	5.91	0.82	0.41
TiO_2	1.63	0.60	0.23
MgO	1.08	0.58	0.07
K_2O	1.94	1.78	0.05
Na_2O	0.23	-	0.10
MnO	0.05	-	-
SrO	0.04	-	-
ZnO	0.03	-	-
SO_3	0.45	-	-

2.2. Slurry preparation and post-processing.

Four batch compositions were used to study where the weight percentage of fly ash, china clay, and alumina of each batch composition is presented in Table 2.

Table 2. Batch compositions of raw materials.

Batches	Raw Materials		
	Fly Ash (wt.%)	China Clay (wt.%)	Alumina (wt.%)
C1	60	20	20
C2	55	22.5	22.5
C3	50	20	30
C4	45	15	40

Oxide compositions of all the batches are present in Table 1. From the introduction, mullite has stoichiometry $3Al_2O_3.2SiO_2$ where 72.8 wt.% is alumina, and 28.8 mass% is silica when reacting at high-temperature mullite crystals form. The figure shows a progressive increase in wt.% of alumina and silica towards the weight % of stoichiometric mullite from batch C1 to C4. The level of other mineralizing oxides, like TiO_2, Fe_2O_3, CaO, Na_2O, K_2O, and MgO, is diminishing from batch C1 to C4.

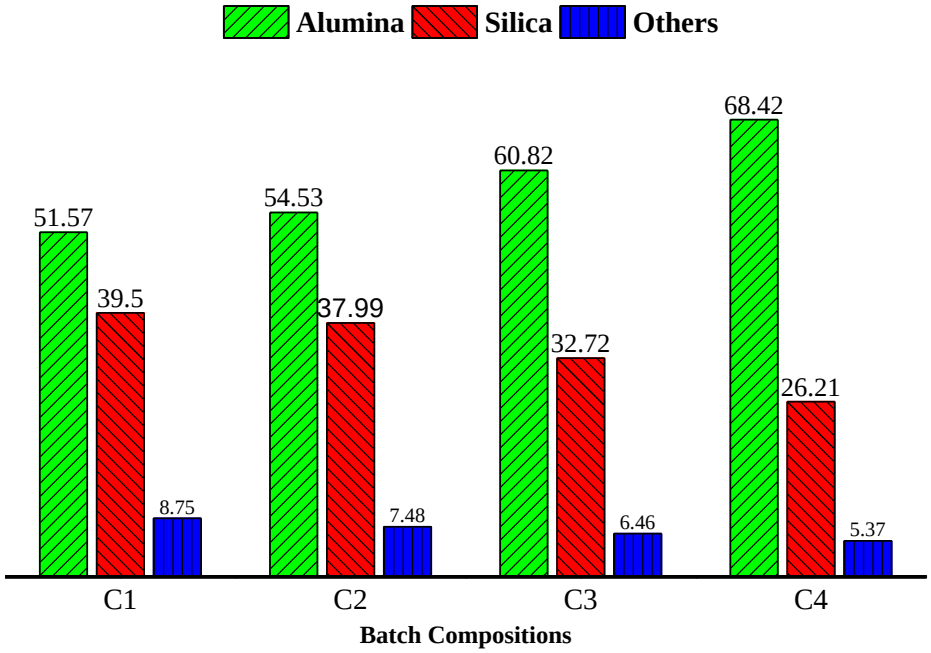

Figure 1. Oxide compositions of experimental batches (C1, C2, C3, and C4) in weight percentages.

In this present work, the organic gelling agent albumin is used to consolidate the powder particles. Figure 2 shows the graphical representation of the albumin gel casting process. The ceramic slurry was made up of a solid loading of 50 vol.%, albumin of 20 vol.%, and 30 vol.% of distilled water. Additives such as antifoaming agent 1-Octanol (5 ml per 100 ml of albumin) are used to get foam-free slurry, and ammonium polyacrylate (1 wt.%) is used as a dispersant [48]. As per calculations, the mixtures of all the raw materials, including powders, albumin, distilled water, and additives, were taken and then milled in a horizontal pot mill for 24 hours using a zirconia ball of diameter 3 mm as milling media. After pot milling, the ceramic slurry was cast into a plastic mold, where petroleum jelly was used as a mold release agent. The plastic mold was covered by aluminum foil and subjected to a preheated hot air oven at 80°C for an hour to gelation. The mold was left to cool for the whole night, and then samples dried up to 100°C in the oven. All the green bodies were subjected to binder burnout in a muffle furnace at 900°C with a heating rate of 2.5°C/minutes. Finally, the sintering operation was carried out at 1200°C, 1250°C, and 1300°C for 2 hours with a heating rate of 3°C/min. Figure 3(a-b) shows the images of the green body samples dried up to 100°C and samples sintered at 1300°C for two hours, respectively.

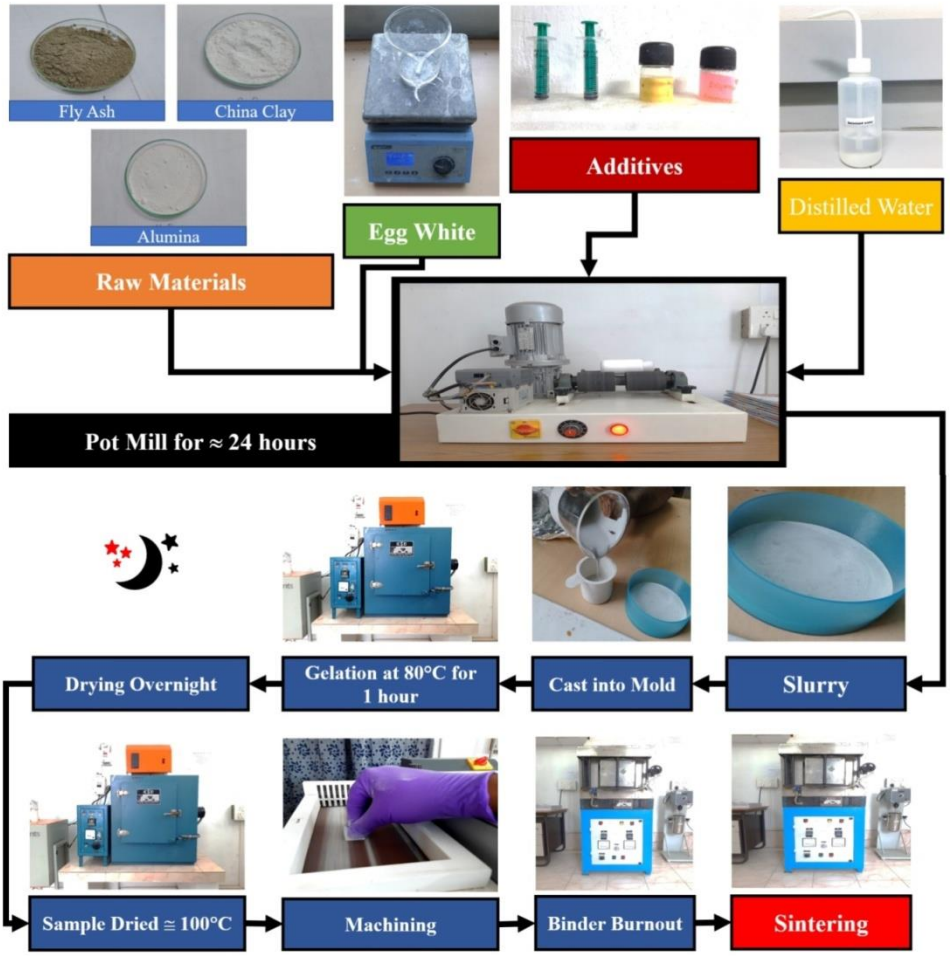

Figure 2. Pictorial representation of the albumen gelcasting process.

The stability of ceramic slurry was characterized by measuring zeta potential by a zeta potential measurement instrument (Model: Litesizer 500, make: Anton Paar). The experiment was conducted at 25°C with 20 scans. Calorimetric study of the binder and binder containing slurry was carried out by differential scanning calorimetry (DSC-Model: DSC 214 Polyma, make: Netzsch), with a heating rate of 5°C/min a nitrogen atmosphere. Before the test, eggs

were collected from the local market and broken by using a tweezer to collect the fresh albumin (white portion only) in a beaker, followed by mixing slowly by a magnetic stirrer for 2 hours to get a homogeneous mixture.

2.3. Characterization of green samples and sintered samples

The fracture surfaces of the green specimens were characterized by using Carl Zeiss make field emission scanning electron microscopy. Physical properties of sintered samples, such as linear shrinkage, density, percentage porosity, and percentage water absorption, were also measured. The fractured surfaces of sintered specimens were observed using Carl Zeiss make field emission scanning electron microscopy.

3. Results and Discussion

3.1. Morphology study of starting powders by FESEM

The morphology and surface texture of fly ash, china clay, and alumina powder used in this investigation is shown in Figure 4 (a-f). Figure 4 (a-b) shows that significant numbers of fly ash particles are spherical, and some of the particles were angular and irregularly agglomerated to nearby particles. The morphology and surface texture of china clay particles is shown in Figure 4 (c-d). The high magnification FESEM micrograph 4 (d) reveals that the flake-shaped particles were arranged in a face-to-face pattern.

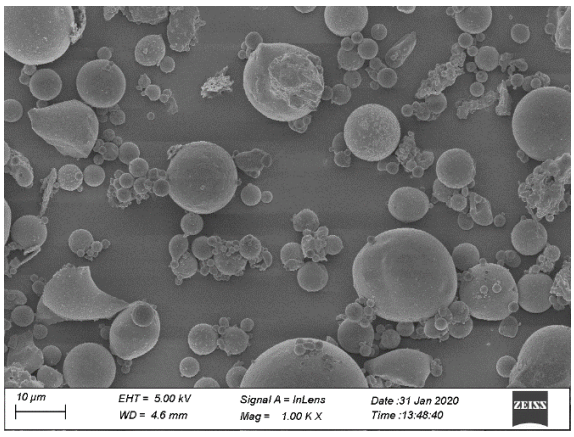

(a)

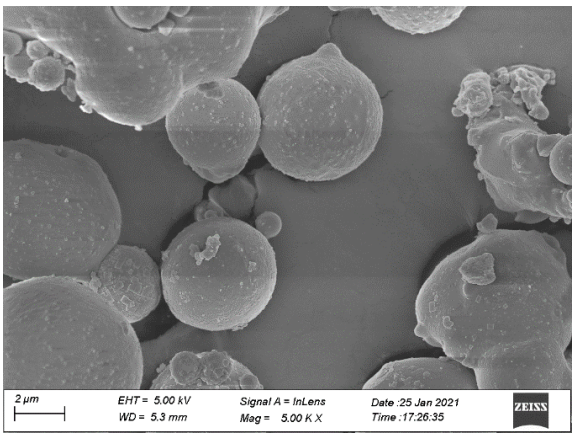

(b)

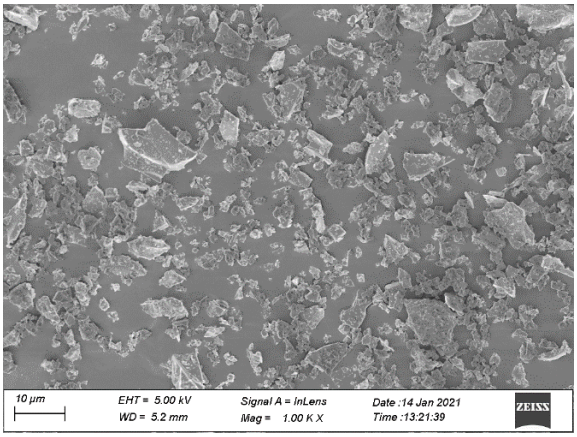

(c)

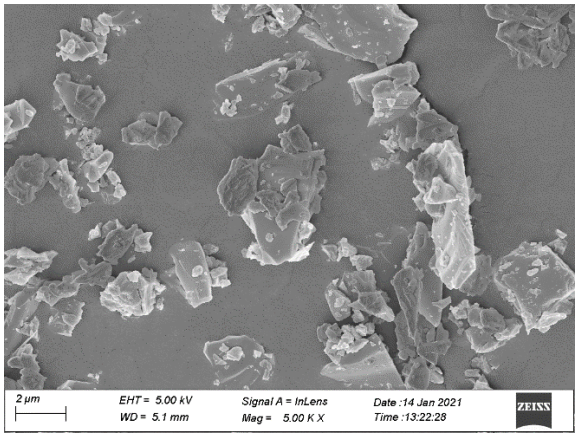

(d)

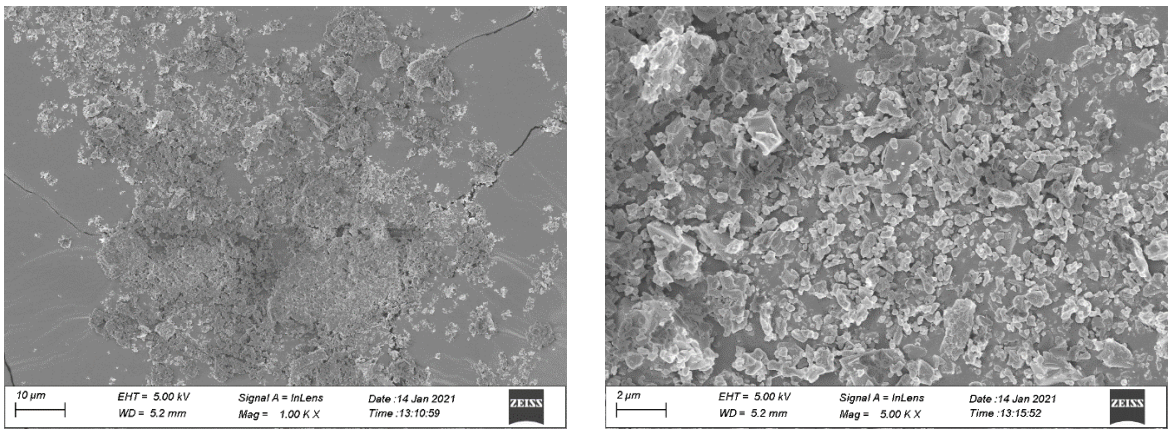

(e) (f)

Figure 4. FESEM micrographs of **(a, b)** fly ash powder, **(c, d)** china clay powder, and **(e, f)** alumina powder.

Further, it can be seen that some particles are a well pseudohexagonal pattern along with some agglomerated, which look like a plate shape as reported in the previous literature [52]. Figure 4 (e-f) shows the morphology of the alumina powder, which is an angled, irregular heterogeneous polygon shape with soft agglomerations.

3.2. Characterization of ceramic slurry.

The stability of ceramic slurries was analyzed by measuring the zeta potential value as shown in Figure 5. The zeta potential calculation is based on the velocity and direction of particles in the solution affected by a known electric field [53]. The zeta potential worth describes the surface charge of the suspended particles [54]. This is utilized to dissect the conceivable degree of the slurry's flocculation or de-flocculation and colloidal solidness.

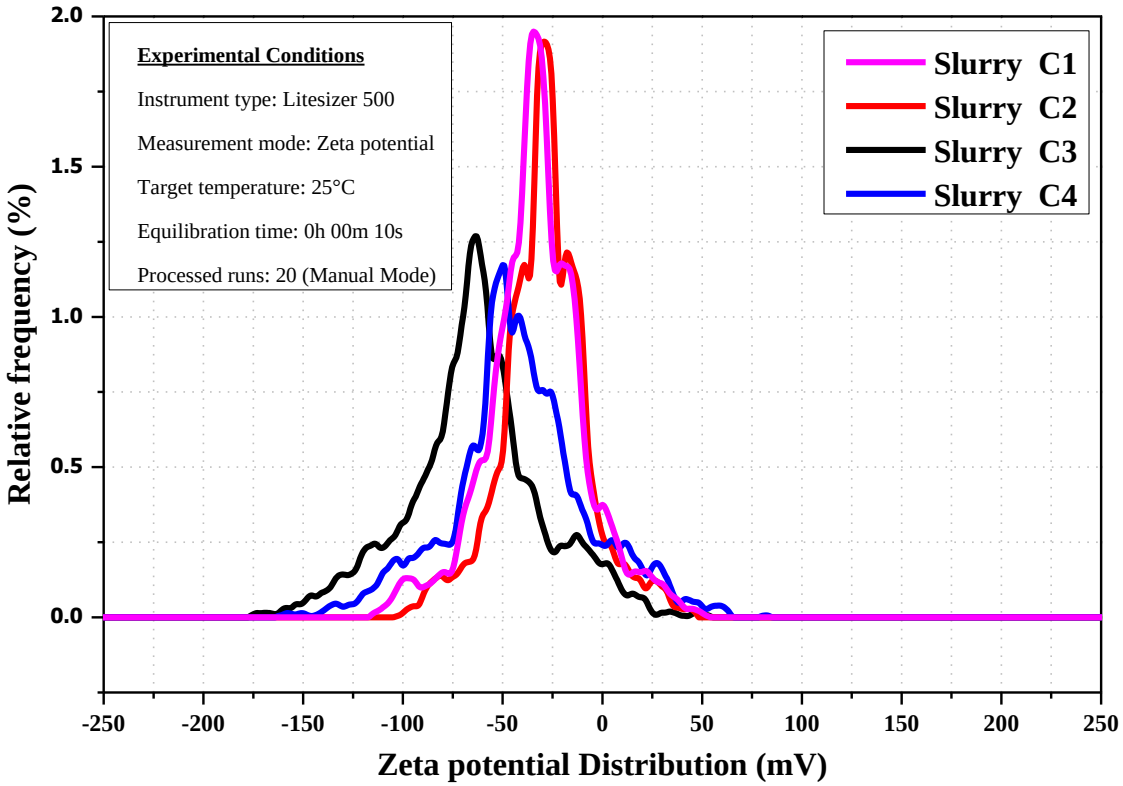

Figure 5. Zeta potential graphs of all the slurries.

It has been reported that the zeta potential value indicates the colloidal stability of the ceramic slurry. If the zeta potential value lies between +25 mV or -25 mV, the slurry is unstable due to settling ceramic powder particles for gravitational force [55,56]. In this present investigation, the slurry's zeta potential is greater than -25 mV. This affirms that slurries are profoundly stable, well dispersed, and contain non-agglomerated particles. Figure 5 shows that slurry made by batch composition C1 has a height zeta value of -63.7 mV, and C2, C3, and C4 have -49.2, -33.6, and -31.2 mV, respectively. Zeta potential value keeps reducing from C1 to C4 because of gradually increasing alumina content in batches [57].

The DSC method has been demonstrated to contemplate albumin and albumin-containing slurry thermal behavior and examine the structural changes [58]. The DSC curves of pure albumin and albumin-containing slurry are shown in Figure 6. The DSC curve of fresh albumin shows sharp peaks at 112°C due to albumin denaturation means the unfolding of the protein chain and the more heat-stable form of albumin called S-ovalbumin (type of protein present in albumin). The curve obtained with pure albumin confirms this interpretation. The obtained result and the proposed interpretation concur with information available in various works of literature [59,60]. On the other hand, the endothermic peak for albumin-containing slurry shifts toward a lower temperature at 80°C, which confirms the gelling temperature.

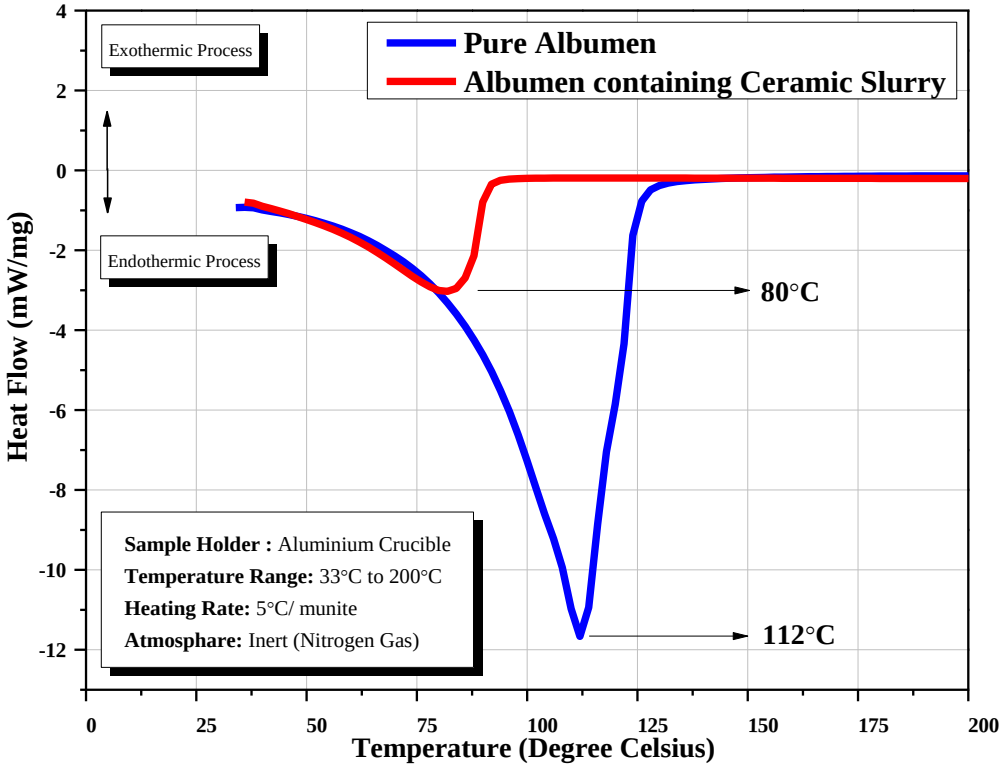

Figure 6. Differential scanning calorimetric curves of pure albumen and albumen containing slurry.

3.3. Microstructural features study of green samples

The fracture surface of green samples (C4 batch composition) dried up to 100°C is shown in Figure 7 (a-d). It can be seen that green bodies exhibit homogeneous microstructure and good packing of particles with some porosity when solid loading is under 50 vol.%. There is no evidence of any crack in the green body microstructures. This could be due to the stable and well-dispersed ceramic slurry. Further, it has been observed that the green sample prepared by the gel casting process provides excellent green strength for handling and machining.

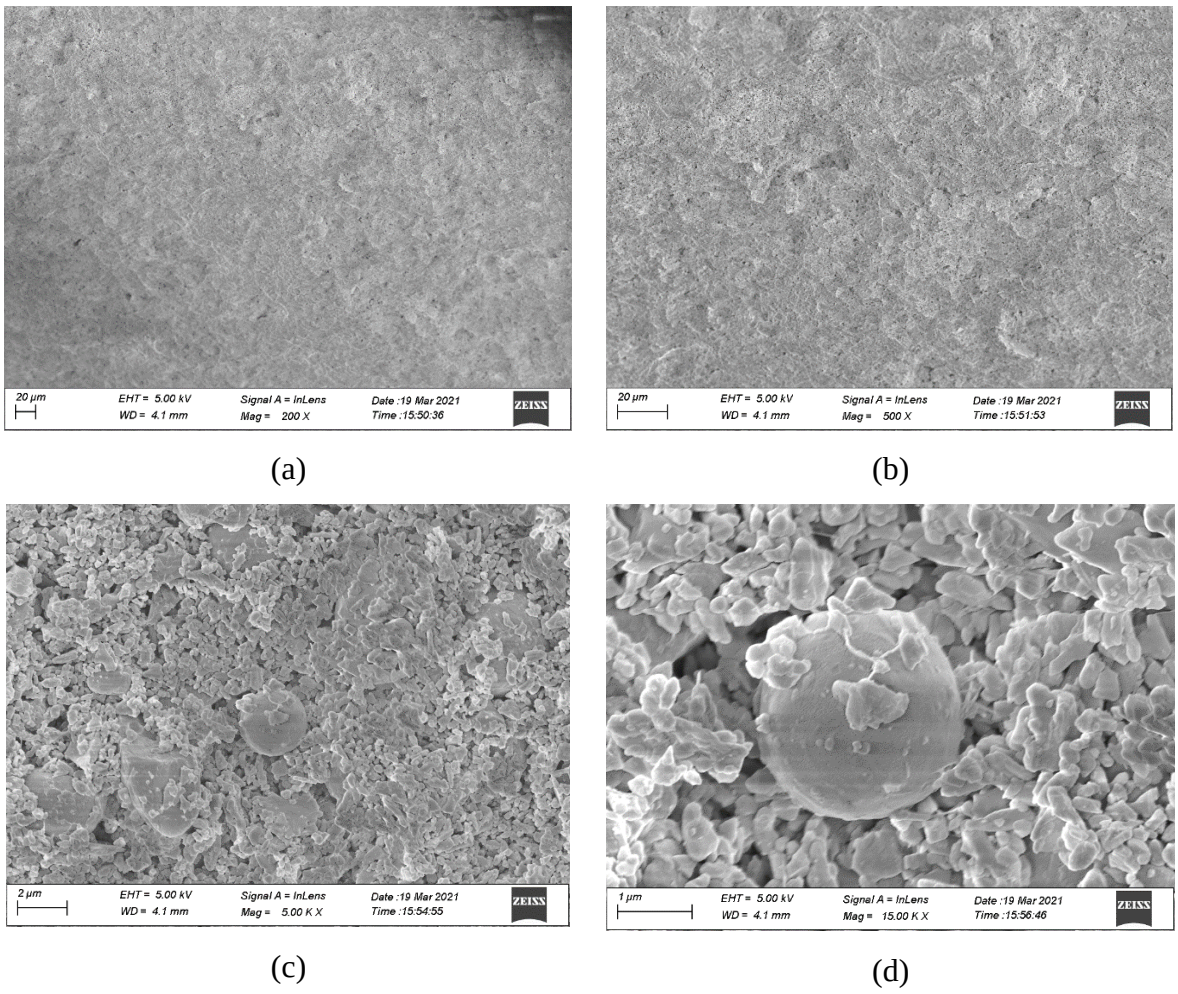

Figure 7. (a-d). The fracture surface of green samples (C4 batch composition) dried up to 100°C.

3.4. Physical properties of sintered samples

Figure 8. (a-d) illustrates physical properties such as density, porosity, linear shrinkage, and water absorption of sintered samples. The linear shrinkage and density increase with the sintering temperatures from 1200°C to 1300°C, while the water absorption and porosity value have the opposite trend. In this study, the green samples sintered at 1300°C shows optimal sintering properties, with a density of 90.85 %, water absorption of 0.10 %, linear shrinkage of 15.70 %, and porosity of 0.68 %. From the above data, as expected, with an increase in sintering temperature from 1200(C) to 1300(C), the densification process in the green ceramic body has increased. There is no sign of over-sintering, as seen in the photographs of the sintered sample (Figure 3b) and the physical properties data (Figure 8a-d). Over-sintering also leads to a decrease in density, linear shrinkage, and an increase in water absorption and porosity value. For this batch composition, the over-sintering temperatures may be above 1300°C. Previous literature on the sintering process indicates that the over-sintering of the green ceramic leads to a sharp increase in flow ability leading to micropores within the microstructure [26]. Further, it has been mentioned that excess high-temperature sintering is associated with abnormal grain growth leading to minimizing the strength values [27].

As per the current data and results analysis, the sintering for all batch compositions is believed to be liquid phase sintering. During the liquid phase sintering of fly ash, alumina, and silica powder mix compositions ceramic green body, the dissolution of the alumina in the silica-rich low-temperature eutectic melt phase formed by Fe_2O_3, TiO_2, CaO, MgO, Na_2O that are

present in fly ash powder and china clay powder. That could be the possible reason for the minimizing internal micropores and nucleation and growth of mullite crystal in the sintered ceramics microstructure [29].

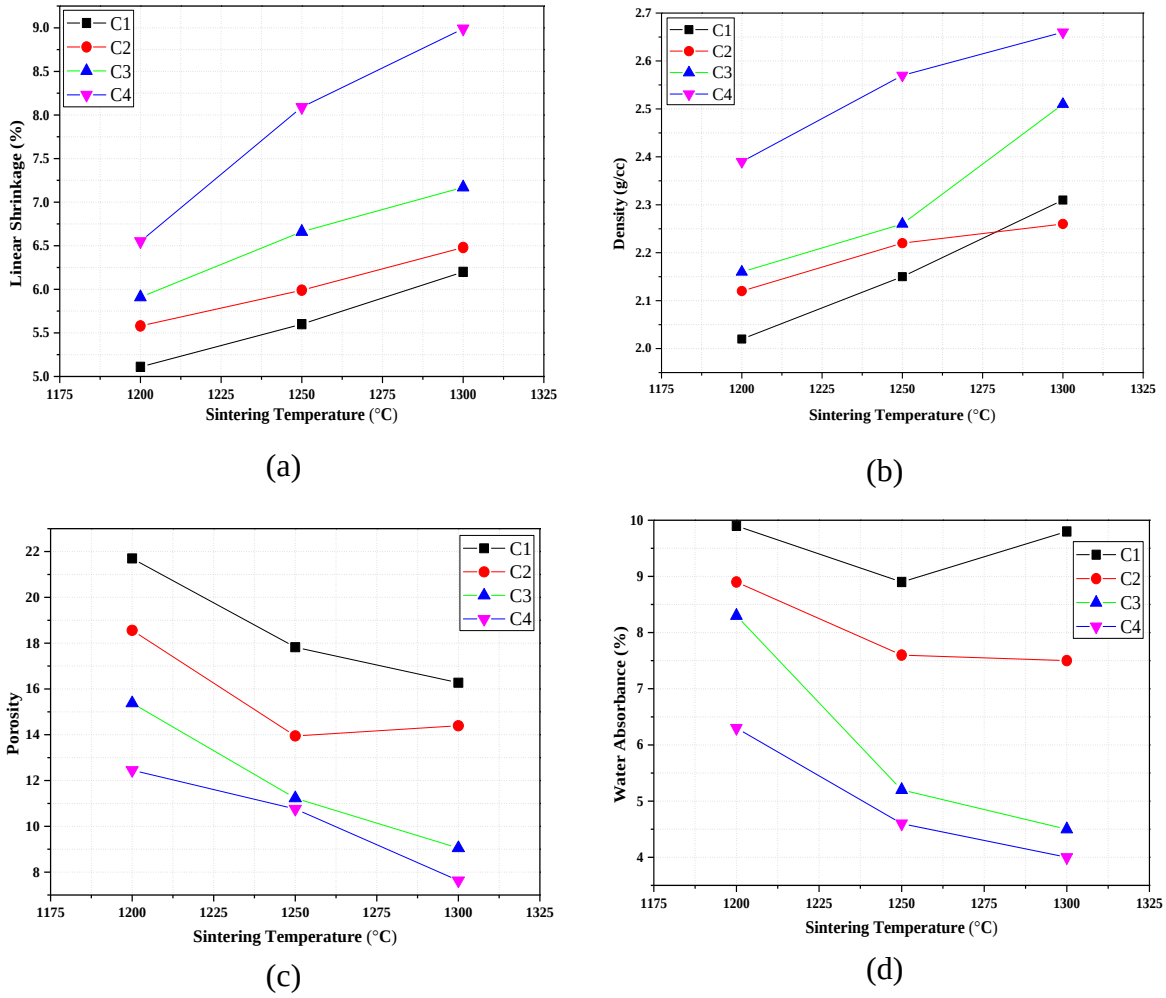

Figure 8. Physical properties of sintered sample, **(a)** linear shrinkage, **(b)** bulk density, **(c)** percent porosity, **(d)** water absorption.

3.5. Microstructural feature study of sintered samples.

Figure 9 represents the FESEM fractography of all the batches sintered at 1300°C. Fractography exhibits porous microstructure for the batch C1 (Figure 9a-d) and C2 (Figure 10a-d) sintered samples. On the other hand, the sintered sample of the batch composition C3 (Figure 11a-d), and C4 (Figure 12a-d), shows less porosity and uniform and dense microstructure compared to C1 and C2.

Further, micrographs exhibit some unreacted powder particles in the sintered sample prepared from all the batch compositions indicating a bit higher temperature sintering required for complete densification. Although mullite is present in all the batch compositions, the extent of mullite formation was increased from C1 composition to C4 composition. FESEM fractography (Figure 12d) of C4 batch composition sintered at 1300°C exhibits mullite crystals as a fine needle with an average length of 1.52 µm and thickness of 0.23 µm.

Densification during the sintering process occurs because of the generation of liquid, which transforms into a glassy phase. According to the Al_2O_3–SiO_2 binary phase diagram, the liquid phase can be formed at above eutectic temperature (1590 ± 10°C) [42]. In this present investigation, a liquid glassy phase was found at a relatively low temperature of 1300°C.

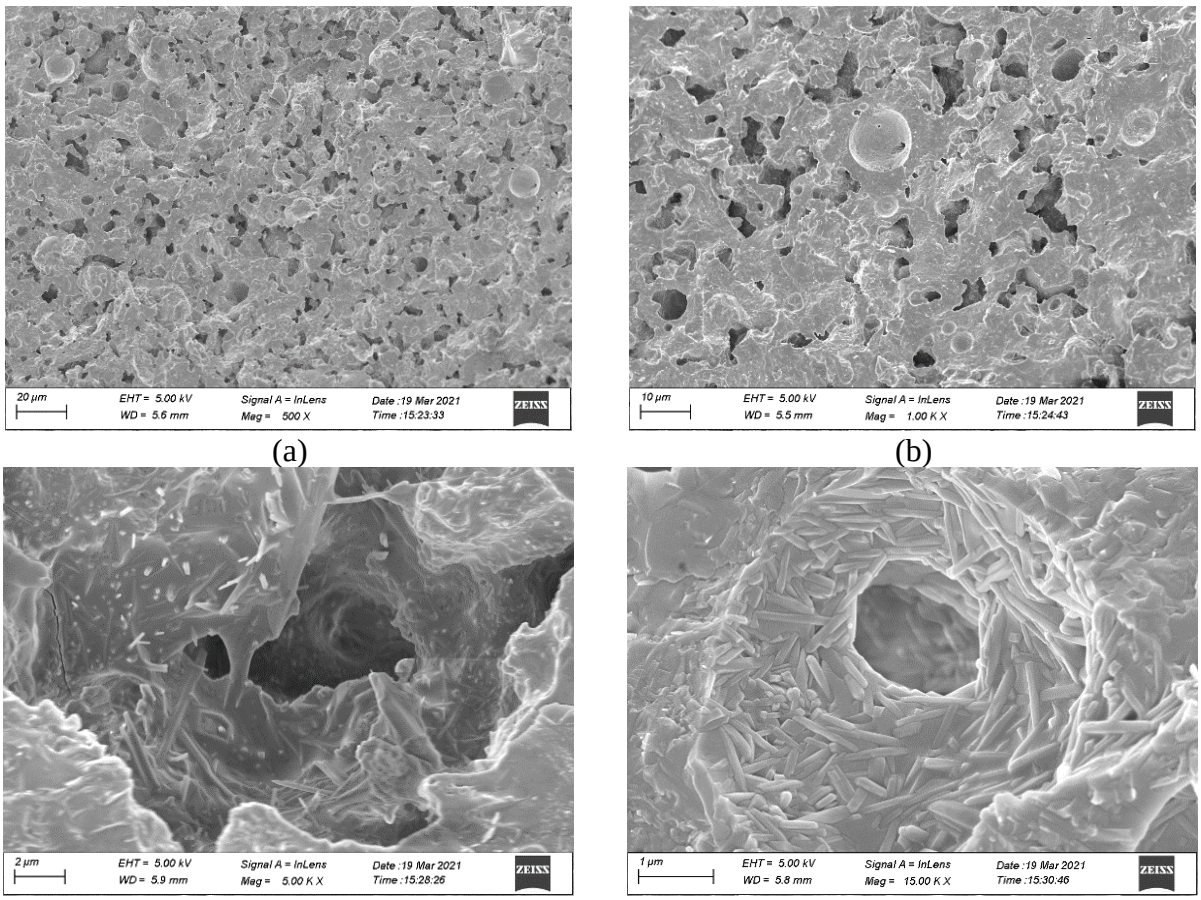

Figure 9. (a-d) FESEM micrographs of fractured surfaces of the C1 batch composition samples sintered at 1300°C for two hours.

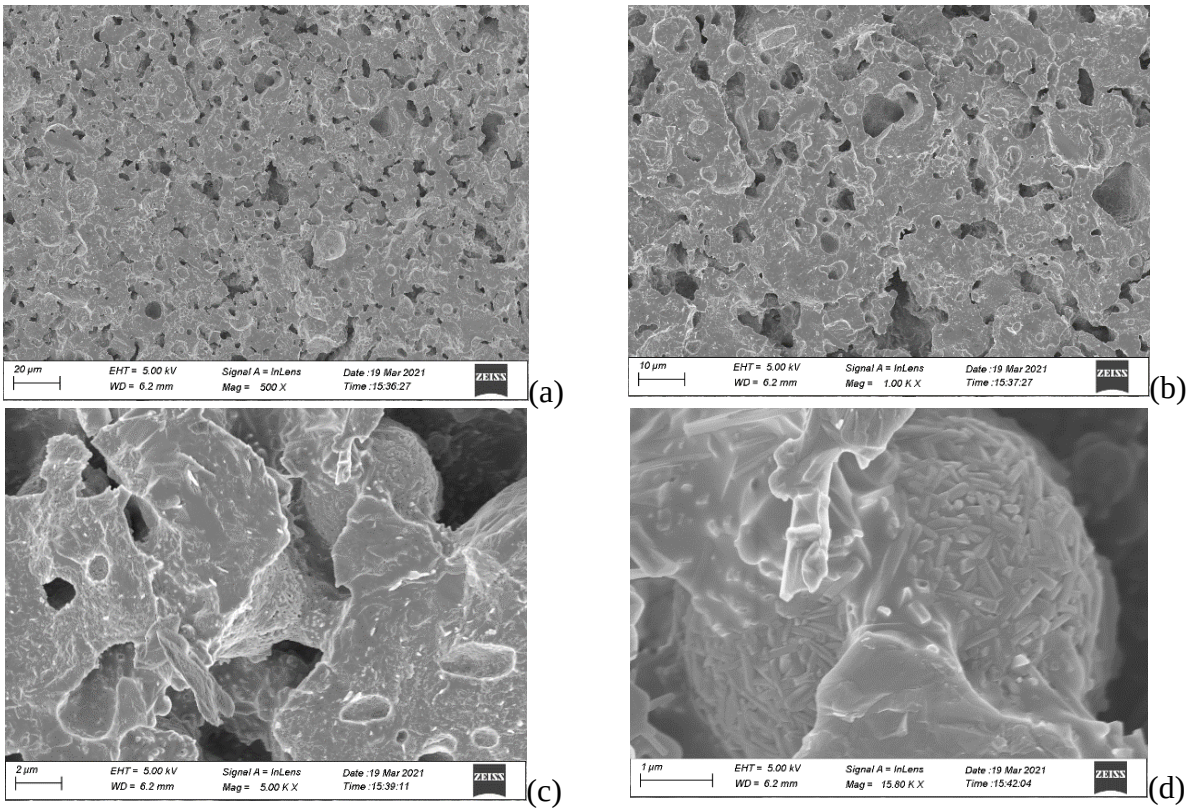

Figure 10. (a-d) FESEM micrographs of fractured surfaces of the C2 batch composition samples sintered at 1300°C for two hours.

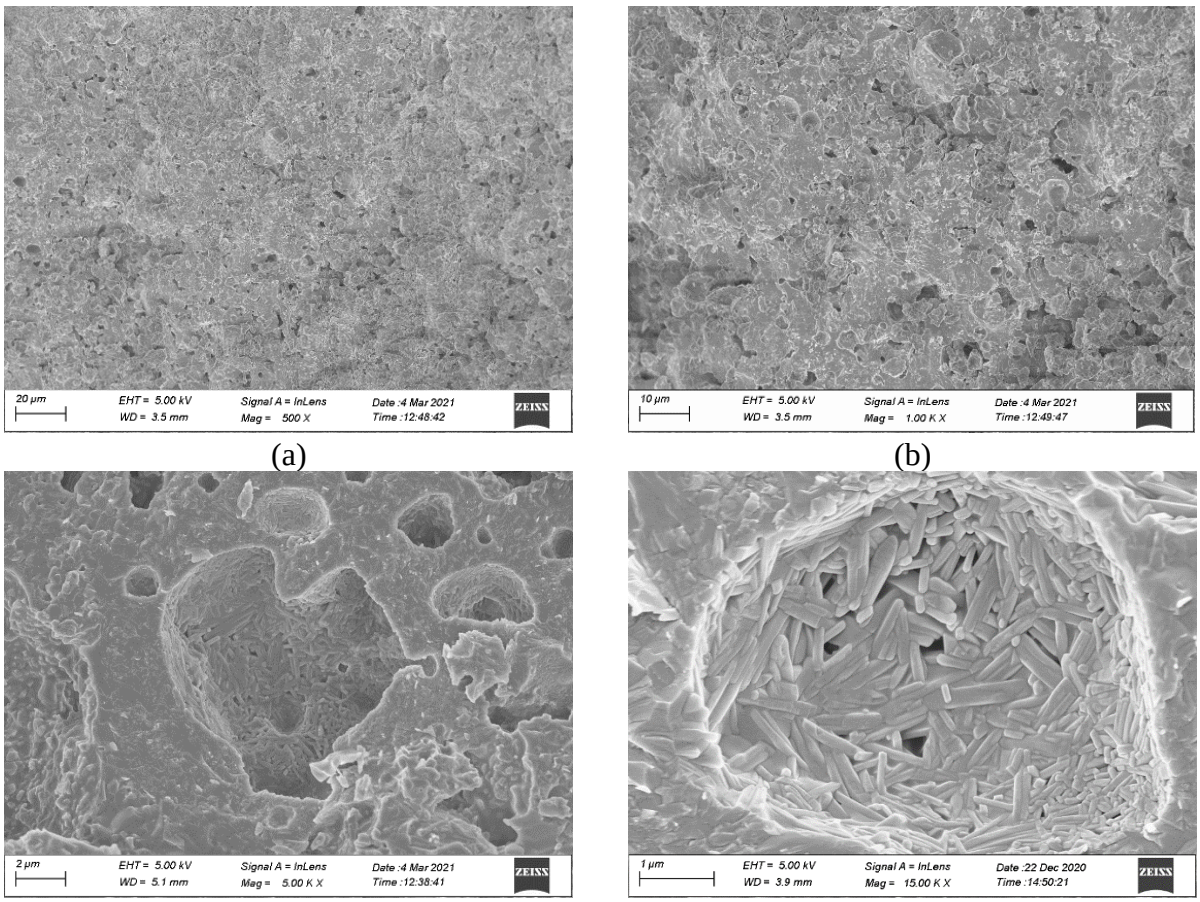

Figure 11. (a-d) FESEM micrographs of fractured surfaces of the C3 batch composition samples sintered at 1300°C for two hours.

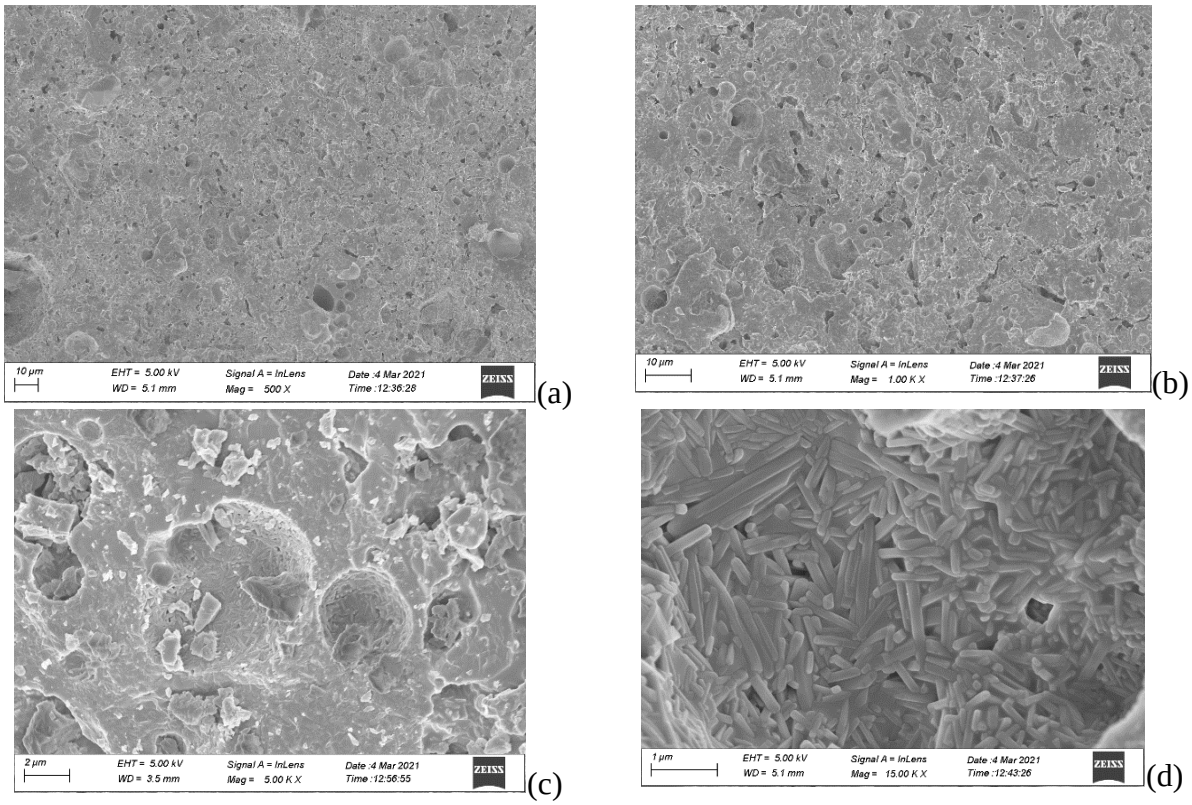

Figure 12. (a-d) FESEM micrographs of fractured surfaces of the C4 batch composition samples sintered at 1300°C for two hours.

4. Conclusion

In this present research work, mullite ceramics were fabricated by the gel casting process, and the concussions are as follows: Albumin can consolidate ceramic powder particles, which form highly loaded aqueous slurries (50 vol. %) that exhibit good homogeneity in the green body; The mullite ceramic sample (C4 – 45 wt.% fly ash, 15 wt.% china clay, and 40 wt.% alumina), which was sintered at 1300°C, exhibits the highest density of 2.66 g/cc, lowest water absorption of 4%, less porosity of 7.63 % and linear shrinkage is about 8.99 % obtained; FESEM fractured surface of sintered samples shows needle-shaped mullite crystals for all the batch compositions, where batch composition C4 exhibits less porosity compared to other batch composition samples and produces a better interlocking of mullite crystals.

The use of albumin as a binder provides many advantages, such as very low cost, availability, biodegradable, and non-toxic as well.

Funding

This research received no external funding.

Acknowledgments

The authors would like to thank Central Instrumentation Center, Tripura University (A Central University), Agartala, Tripura, India, Central Instrumentation Facility and Centre for the Environment, Indian Institute of Technology, Guwahati, Assam, India, for the FESEM and Zeta potential facility, respectively.

Conflicts of Interest

The authors declare no conflict of interest.

References

1. Roy, R.; Das, D.; Rout, P.K.; A Review of Advanced Mullite Ceramics. *Engg. Sci.* **2022**, *18*, 20-30, https://doi.org/10.30919/es8d582.
2. Roy, R.; Das, D.; Rout, P.K. Fabrication of Mullite Ceramic by Using Industrial Waste, 1st ed., Smart Cities: Concepts, Practices, and Applications. *CRC Press*, **2022**, 285-291, https://doi.org/10.1201/9781003287186-13.
3. Schneider, H.; Fischer, R.X.; Schreuer, J. Mullite: Crystal Structure and Related Properties. *J. Am. Ceram. Soc.* **2015,** *98*, 2948–2967, https://doi.org/10.1111/jace.13817.
4. Sadik, C.; El Amrani, I.E.; Albizane, A. Processing and characterization of alumina-mullite ceramics. *J. Asian Ceram. Soc.* **2014**, *2*, 310–316, https://doi.org/10.1016/j.jascer.2014.07.006.
5. Obada, D.O.; Dodoo-Arhin, D.; Dauda, M.; Anafi, F.O.; A.S. Ahmed, O.A. Ajayi, I.A. Samotu, Effect of mechanical activation on mullite formation in an alumina-silica ceramics system at lower temperature. *World J. Eng.* **2016**, *13*, 288–293, https://doi.org/10.1108/WJE-08-2016-039.
6. Anggono, J. Mullite Ceramics: Its Properties Structure and Synthesis, Mullite Ceram. *Its Prop. Struct. Synth.* **2005**, *7*, 1–10, https://doi.org/10.9744/jtm.7.1.pp.1-10.
7. Yuan, W.; Kuang, J.; Huang, Z.; Yu, M. Effect of aluminum source on the kinetics and mechanism of mullite preparation from kaolinite. *Chem. Phy. Lett.* **2022**, *787*, 139242, https://doi.org/10.1016/j.cplett.2021.139242.
8. Tabit, K.; Borja, W.; Saâdi, L.; Waqif, M. Low-temperature synthesis of mullite-based ceramics from Moroccan naturally occurring andalusite and marble waste. *Int J Appl Ceram Technol.* **2021**, *19*, 1274-1280, https://doi.org/10.1111/ijac.13942.
9. Barrientos-Hernández, F.R.; Pérez-Labra, M.; Lobo-Guerrero, A.; Reyes-Pérez, M.; Juárez-Tapia, J.C.; Hernández-Ávila; J.; Cardoso-Legorreta, E.; Hernández-Lara, J.P. Effect of Particle Size and Sintering

Temperature on the Formation of Mullite from Kyanite and Aluminum Mixtures. *Adv. Mater. Sci. Eng.* **2021**, *2021*, 1-13, https://doi.org/10.1155/2021/6678297.
10. Xiao, Z.; Wang, W.; Li, X.; Zhang, L.; Zhang, T.; Gao, M.; Kong, L.B.; Zho, K.; Liu, Y. Progress in fabrication and characterization of mullite whiskers. *J. Micromech. Mol. Phys.* **2021**, *6*, 1-28, https://doi.org/10.1142/S242491302150003X.
11. Ji, H.; Mi, X.; Tian, Q.; Liu, C.; Yao, J.; Ma, S.; Zeng, G. Recycling of mullite from high-alumina coal fly ash by a mechanochemical activation method: Effect of particle size and mechanism research. *Sci. Total Environ*. **2021**, *784*, 1-8, https://doi.org/10.1016/j.scitotenv.2021.147100.
12. Xi Yue; Yong Li; Chenhong Ma; Qingyao Zheng; Xiaofang Wu; Bin Li. Novel process for synthesizing fused mullite from titanium-rich medium/low grade or waste bauxite (2022). *Ceram. Int.* **2022**, *48*, 8228-8234, https://doi.org/10.1016/j.ceramint.2021.12.027.
13. R.M. Khattab; H.H. Abo-Almaged; H.E.H. Sadek. Effects of some extracted oxides on silica fume waste for mullite preparation: Physical, mechanical, optical, magnetic, and dielectric properties, *Mater. Chem. and Phy*. **2022**, *281*, 125880, https://doi.org/10.1016/j.matchemphys.2022.125880.
14. S. Agrawal; N. Dhawan. Evaluation of microwave acid baking on Indian red mud sample, *Miner. Eng.* **2021**, *160*, 106686, 1-5, https://doi.org/10.1016/j.mineng.2020.106686.
15. A. Christogerou; P. Lampropoulou; E. Panagiotopoulos. Increase of frost resistance capacity of clay roofing tiles with boron waste addition, *Constr. Build. Mater.* **2021**, *280*, 122493, https://doi.org/10.1016/j.conbuildmat.2021.122493.
16. Öztürk, S.; Akpınar, M.; Tığ. Effect of calcined colemanite addition on properties of porcelain tile, *J. Aust. Ceram. Soc*. **2022**, *58*, 321–331, https://doi.org/10.1007/s41779-021-00674-2.
17. D. Das P.K.; Rout. Synthesis, Characterization and Properties of Fly Ash Based Geopolymer Materials, *J. Mater. Eng. Perform.* **2021**, *30*, 3213–3231, https://doi.org/10.1007/s11665-021-05647-x.
18. A.S. Saurabh Attarde; Sagar Marathe. Utilization of fly ash in construction industries for environment management, *Int. J. Environ. Sci.* **2014**, *3*, 117–121, https://doi.org/10.1088/1757-899X/601/1/012023.
19. M. Basu; M. Pande; P.B.S. Bhadoria, S.C. Mahapatra. Potential fly-ash utilization in agriculture: *A global review*, *Prog. Nat. Sci*. **2009**, *19*, 1173–1186, https://doi.org/10.1016/j.pnsc.2008.12.006.
20. S. Wang; C. Zhang; J. Chen. Utilization of Coal Fly Ash for the Production of Glass-ceramics With Unique Performances: *A Brief Review*, *J. Mater. Sci. Technol.* 2**014**, *30*, 1208–1212, https://doi.org/10.1016/j.jmst.2014.10.005.
21. D. Das; P.K. Rout. Synthesis and Characterization of Fly Ash and GBFS Based Geopolymer Material, *Biointerface Res. Appl. Chem.* **2021**, *11*, 14506–14519, https://doi.org/10.33263/BRIAC116.1450614519.
22. D. Das; P.K. Rout. Utilization of thermal industry waste: From trash to cash, Carbon – Sci. *Technol*. **2019**, *11*, 43–48, https://www.researchgate.net/publication/334454088_Utilization_of_thermal_industry_waste_From_trash_to_cash.
23. D. Das; A.P Das; P.K. Rout. Effect of Slag Addition on Compressive Strength and Microstructural Features of Fly Ash Based Geopolymer, Effect of slag addition on compressive strength and microstructural features of fly ash based geopolymer, In Circular economy in the construction industry, 1st ed, S.K. Ghosh; B.G. Mahapatra; S.K. Ghosh; R.L. Mersky; eds;. CRC Press, Boca Raton, **2021**, 61–68, https://doi.org/10.1201/9781003217619-9.
24. Y. Zhao; B. Zhou; P. Qiu; Y. Fan; Q. Zheng; W. Luo; X. Cheng; L. Wang; W. Jiang. Ultra-low temperature preparation of mullite glass-ceramics with high transparency sintered from EMT-type zeolite, J. *Am. Ceram. Soc.* **2021**, *104*, 3158–3166, https://doi.org/10.1111/jace.17751.
25. N. Suriyanarayanan; K. V Kannan Nithin; E. Bernardo. Mullite glass ceramics production from coal ash and alumina by high temperature plasma, *J. Non-Oxide Glas*. **2009**, *1*, 247–260, https://www.researchgate.net/publication/237330407_Mullite_glass_ceramics_production_from_coal_ash_and_alumina_by_high_temperature_plasma.
26. J.S. Jung; H.C. Park. Mullite ceramics derived from coal fly ash, J. Mater. Sci. Lett., **2001**, *20*, 1089–1091, https://doi.org/10.1023/A:1010934728570.
27. H. Tan. Preparation of mullite whiskers from coal fly ash using sodium sulfate flux, Int. J. Miner. Process. **2011**, *100*, 188–189. https://doi.org/10.1016/j.minpro.2011.05.008.
28. Y. Dong; J. Diwu; X. Feng; X. Feng; X. Liu; G. Meng. Phase evolution and sintering characteristics of porous mullite ceramics produced from the flyash-Al(OH)3 coating powders. *J. Alloys Compd.* **2008**, *460*, 651–657, https://doi.org/10.1016/j.jallcom.2007.06.043.

29. Y. Li; J. Lu; Y. Zeng; Z. Liu; C. Wang. Preparation and of mullite powders from coal fly ash by the mullitization and hydrothermal processes, Mater. *Chem. Phys.* **2018**, *213*, 518–524, https://doi.org/10.1016/j.matchemphys.2018.04.056.
30. A. Mondal; S. Maitra; S. Chandra; N.K. Mitra. Alumina-mullite composites through interaction of bauxite and fly ash, Trans. *Indian Ceram. Soc.* **2008**, *67*,81–85, https://doi.org/10.1080/0371750X.2008.11078645.
31. J. Cao; X. Dong; L. Li; Y. Dong; S. Hampshire. Recycling of waste fly ash for production of porous mullite ceramic membrane supports with increased porosity. *J. Eur. Ceram. Soc*. **2014**, *34*, 3181–3194, https://doi.org/10.1016/j.jeurceramsoc.2014.04.011.
32. B. Ma; C. Su; X. Ren; Z. Gao; F. Qian; W. Yang; G. Liu; H. Li; J. Yu; Q. Zhu. Preparation and properties of porous mullite ceramics with high-closed porosity and high strength from fly ash via reaction synthesis process. *J. Alloys Compd*. **2019**, *803*, 981–991, https://doi.org/10.1016/j.jallcom.2019.06.272.
33. A.K. Yadav; L. Farheen; S. Bhattacharyya. Preparation of low-cost porous mullite balls from kaolin and alumina using naphthalene as pore-former. *AIP Conf. Proc.* 2115, **2019**. https://doi.org/10.1063/1.5112856.
34. X. Mao; S. Shimai; M. Dong; S. Wang. Gelcasting of alumina using epoxy resin as a gelling agent. *J. Am. Ceram. Soc.* **2007**, *90*, 986–988, https://doi.org/10.1111/j.1551-2916.2007.01492.x.
35. A.C. Young; O.O. Omatete; M.A. Janney; P.A. Menchhofer; Gelcasting of Alumina. *J. Am. Ceram. Soc*. **1991**, *74*, 612–618, https://doi.org/10.1111/j.1151-2916.1991.tb04068.x.
36. J.M. Tulliani; E. Bemporad; M. Sebastiani; G. Pulci; J. Tirillò; C. Bartuli. Dense and cellular zirconia produced by gel casting with agar: Preparation and high temperature characterization. *J. Nanomater*. **2013**, https://doi.org/10.1155/2013/108076.
37. R. Mouazer; I. Thijs; S. Mullens; J. Luyten. SiC foams produced by gel casting: Synthesis and characterization. *Adv. Eng. Mater.* **2004**, *6*, 340–343, https://doi.org/10.1002/adem.200400009.
38. W. Wan; J. Yang; J. Zeng; L. Yao; T. Qiu. Aqueous gelcasting of silica ceramics using DMAA. *Ceram. Int.* **2014**, *40*, 1257–1262, https://doi.org/10.1016/j.ceramint.2013.06.048.
39. A. Yang; C.A. Wang; R. Guo; Y. Huang; C.W. Nan. Porous PZT ceramics with high hydrostatic figure of merit and low acoustic impedance by TBA-based gel-casting process. *J. Am. Ceram. Soc*. **2010**, *93*, 1427–1431, https://doi.org/10.1111/j.1551-2916.2009.03585.x.
40. S. Dhar; R.K. Kamboj; M. Pradhan; P. Bhargava. Shape forming of ceramics via gelcasting of aqueous particulate slurries. *Bull. Mater. Sci.* **2002**, *25*, 565–568, https://doi.org/10.1007/BF02710552.
41. Y. Yang; S. Shimai; S. Wang. Room-temperature gelcasting of alumina with a water-soluble copolymer. *J. Mater. Res.* ***2013***, *28*, 1512–1516, https://doi.org/10.1557/jmr.2013.132.
42. R. Chen; C.A. Wang; Y. Huang; L. Ma; W. Lin. Ceramics with special porous structures fabricated by freeze-gelcasting: Using tert-butyl alcohol as a template. *J. Am. Ceram. Soc*. **2007**, *90*, 3478–3484, https://doi.org/10.1111/j.1551-2916.2007.01957.x.
43. F. Chabert; D.E. Dunstan; G. V. Franks. Cross-linked polyvinyl alcohol as a binder for gelcasting and green machining. *J. Am. Ceram. Soc.* **2008**, *91*, 3138–3146, https://doi.org/10.1111/j.1551-2916.2008.02534.x.
44. Y. Jia; Y. Kanno; Z. peng Xie. New gel-casting process for alumina ceramics based on gelation of alginate. *J. Eur. Ceram. Soc*. **2002**, *22*, 911–1916, https://doi.org/10.1016/S0955-2219(01)00513-1.
45. M. Potoczek. Gelcasting of alumina foams using agarose solutions. *Ceram. Int.* **2008**, *34*, 661–667, https://doi.org/10.1016/j.ceramint.2007.02.001.
46. M. Lombardi; V. Naglieri; J.M. Tulliani; L. Montanaro. Gelcasting of dense and porous ceramics by using a natural gelatine. *J. Porous Mater.* **2009**, *16*, 393–400, https://doi.org/10.1007/s10934-008-9212-0.
47. W. Pabst; E. Gregorov; J. Havrda; E. Tanov. Gelatin Casting and Starch Consolidation of Alumina Ceramics. *Ceram. Mater. Components Engines.* **2007**, 587–592, https://doi.org/10.1002/9783527612765.c100.
48. S. Dhara; P. Bhargava. Egg White as an Environmentally Friendly Low-Cost Binder for Gelcasting of Ceramics. *J. Am. Ceram. Soc.* **2001**, *84*, 3048–3050, https://doi.org/10.1111/j.1151-2916.2001.tb01137.x.
49. D. Guo; K. Cai. Gelcasting of Ferroelectric Ceramics: Doping Effect and Further Development. *Adv. Ferroelectr*. **2012**, 209–229, https://doi.org/10.5772/53995.
50. H. Le Ferrand. Magnetic slip casting for dense and textured ceramics: A review of current achievements and issues. *J. Eur. Ceram. Soc.* **2021**, *41*, 24–37, https://doi.org/10.1016/j.jeurceramsoc.2020.08.030.
51. M. Potoczek; A. Zima; Z. Paszkiewicz; A. Ślósarczyk. Manufacturing of highly porous calcium phosphate bioceramics via gel-casting using agarose. *Ceram. Int.* **2009**, *35*, 2249–2254, https://doi.org/10.1016/j.ceramint.2008.12.006.

52. P. Sengupta; P.C. Saikia; P.C. Borthakur. SEM-EDX characterization of an iron-rich kaolinite clay. *J. Sci. Ind. Res*. (India)., **2008**, *67*, 812–818, https://www.researchgate.net/publication/256427436_SEM-EDX_characterization_of_an_iron-rich_kaolinite_clay.
53. S.S. Hakkimane; V.P. Shenoy; S.L. Gaonkar; I. Bairy; B.R. Guru. Antimycobacterial susceptibility evaluation of rifampicin and isoniazid benz-hydrazone in biodegradable polymeric nanoparticles against Mycobacterium tuberculosis H37Rv strain. *Int. J. Nanomedicine.* **2018**, *13*, 4303–4318, https://doi.org/10.2147/IJN.S163925.
54. H. Wu; C. Sun; Y Huang; X. Zheng; M. Zhao; S. Gray; Y Dong. Treatment of oily wastewaters by highly porous whisker-constructed ceramic membranes: Separation performance and fouling models. *Water Res.* **2022**, *211*, 118042, https://doi.org/10.1016/j.watres.2022.118042.
55. L. Wu; J. Zhang; W. Watanabe. Physical and chemical stability of drug nanoparticles, Adv. Drug Deliv. Rev. **2011**, *63*, 456–469, https://doi.org/10.1016/j.addr.2011.02.001.
56. M.C. Smith; R.M. Crist; J.D. Clogston; S.E. McNeil. Zeta potential: a case study of cationic, anionic, and neutral liposomes. *Anal. Bioanal. Chem*. **2017**, *409*, 5779–5787, https://doi.org/10.1007/s00216-017-0527-z.
57. S. Vallar; D. Houivet; J. El Fallah; D. Kervadec; J.M. Haussonne. Oxide slurries stability and powders dispersion: Optimization with zeta potential and rheological measurements. *J. Eur. Ceram. Soc*. **1999**, *19*, 1017–1021, https://doi.org/10.1016/S0955-2219(98)00365-3.
58. M. Ferreira; C. Hofer; A. Raemy. A calorimetric study of egg white proteins. *J. Therm. Anal.* **1997**, *48*, 683–690, https://doi.org/10.1007/BF01979514.
59. J.W. Donovan; C.J. Mapes; J.G. Davis; J.A. Garibaldi. A differential scanning calorimetric study of the stability of egg white to heat denaturation. *J. Sci. Food Agric*. **1976**, *26*, 73–83, https://doi.org/10.1002/jsfa.2740260109.
60. Y. Li; J. Feng; Y. Wang; X. Chen. Preparation of mullite ceramics with fly ash and clay by pickling process. *Int. J. Appl. Ceram. Technol*. **2015**, *12*, E132–E137, https://doi.org/10.1111/ijac.12258.